



A delivery system specifically approaching bone resorption surfaces to facilitate therapeutic modulation of microRNAs in osteoclasts



Jin Liu ^{a, b, c, d, e, 1}, Lei Dang ^{a, b, c, d, e, 1}, Defang Li ^{a, b, c, d, e, 1},
 Chao Liang ^{a, b, c, d, e, f}, Xiaojuan He ^{a, b, g}, Heng Wu ^{a, b}, Airong Qian ^{e, f}, Zhijun Yang ^a,
 Doris W.T. Au ^h, Michael W.L. Chiang ^h, Bao-Ting Zhang ⁱ, Quanbin Han ^a, Kevin K.M. Yue ^a,
 Hongqi Zhang ^a, Changwei Lv ^j, Xiaohua Pan ^k, Jiake Xu ^l, Zhaoxiang Bian ^a, Peng Shang ^f,
 Weihong Tan ^{m, n, o}, Zicai Liang ^{c, p}, Baosheng Guo ^{a, b, c, d, e, f, *}, Aiping Lu ^{a, b, c, d, e, g, *},
 Ge Zhang ^{a, b, c, d, e, f, *}

^a Institute for Advancing Translational Medicine in Bone & Joint Diseases, School of Chinese Medicine, Hong Kong Baptist University, Hong Kong, China

^b Academician Chen Xinzi Workroom for Advancing Translational Medicine in Bone & Joint Diseases, Kunshan RNAi Institute, Kunshan Industrial Technology Research Institute, Kunshan, Jiangsu 215347, China

^c Institute of Integrated Bioinformatic Medicine and Translational Sciences, HKBU Shenzhen Research Institute and Continuing Education, Shenzhen 518057, China

^d Shum Yiu Foon Shum Bik Chuen Memorial Centre for Cancer and Inflammation Research, HKBU Shenzhen Research Institute and Continuing Education, Shenzhen 518057, China

^e Hong Kong Baptist University – Northwestern Polytechnical University Joint Research Centre for Translational Medicine on Musculoskeletal Health in Space, Shenzhen, 518057, China

^f Key Laboratory for Space Bioscience and Biotechnology, Institute of Special Environmental Biophysics, School of Life Science, Northwestern Polytechnical University, Xi'an, 721000, China

^g Institute of Basic Research in Clinical Medicine, China Academy of Chinese Medical Sciences, Beijing, 100700, China

^h Department of Biology and Chemistry, City University of Hong Kong, 999077, Hong Kong, China

ⁱ School of Chinese Medicine, The Chinese University of Hong Kong, Hong Kong SAR, 999077, China

^j Department of Orthopaedics, Xijing Hospital, The Fourth Military Medical University, Xi'an, 710032, China

^k Department of Orthopaedics & Traumatology, Shenzhen People's Hospital, Second Medical College of Ji'nan University, Shenzhen, 518020, China

^l Molecular Lab, School of Pathology and Laboratory Medicine, University of Western Australia, Nedlands, WA 6009, Australia

^m Department of Chemistry, University of Florida, Gainesville, FL 32611-7200, USA

ⁿ Department of Physiology and Functional Genomics, University of Florida, Gainesville, FL 32611-7200, USA

^o Center for Research at Bio/Nano Interface, Shands Cancer Center, University of Florida, Gainesville, FL 32611-7200, USA

^p Institute of Molecular Medicine, Peking University, Beijing, 100871, China

ARTICLE INFO

Article history:

Received 10 October 2014

Received in revised form

28 January 2015

Accepted 1 February 2015

Available online

Keywords:

Targeted delivery system

MicroRNA

Osteoclast

Bone resorption

ABSTRACT

Dysregulated microRNAs in osteoclasts could cause many skeletal diseases. The therapeutic manipulation of these pathogenic microRNAs necessitates novel, efficient delivery systems to facilitate microRNAs modulators targeting osteoclasts with minimal off-target effects. Bone resorption surfaces characterized by highly crystallized hydroxyapatite are dominantly occupied by osteoclasts. Considering that the eight repeating sequences of aspartate (D-Asp₈) could preferably bind to highly crystallized hydroxyapatite, we developed a targeting system by conjugating D-Asp₈ peptide with liposome for delivering microRNA modulators specifically to bone resorption surfaces and subsequently encapsulated antagomir-148a (a microRNA modulator suppressing the osteoclastogenic miR-148a), *i.e.* (D-Asp₈)-liposome-antagomir-148a. Our results demonstrated that D-Asp₈ could facilitate the enrichment of antagomir-148a and the subsequent down-regulation of miR-148a in osteoclasts *in vivo*, resulting in reduced bone resorption and attenuated deterioration of trabecular architecture in osteoporotic mice. Mechanistically, the osteoclast-targeted delivery depended on the interaction between bone resorption surfaces and D-Asp₈. No

* Corresponding authors. Institute for Advancing Translational Medicine in Bone & Joint Diseases, School of Chinese Medicine, Hong Kong Baptist University, Hong Kong, China.

E-mail addresses: borisguo@hkbu.edu.hk (B. Guo), aipinglu@hkbu.edu.hk (A. Lu), zhangge@hkbu.edu.hk (G. Zhang).

¹ Jin Liu, Lei Dang and Defang Li contributed equally to this work.

detectable liver and kidney toxicity was found in mice after single/multiple dose(s) treatment of (D-Asp₈)-liposome-antagomir-148a. These results indicated that (D-Asp₈)-liposome as a promising osteoclast-targeting delivery system could facilitate clinical translation of microRNA modulators in treating those osteoclast-dysfunction-induced skeletal diseases.

© 2015 Elsevier Ltd. All rights reserved.

1. Introduction

Skeletal diseases induced by osteoclast dysfunction are still great clinical challenges [1]. Increasing evidences demonstrated that a series of dysregulated miRNAs within osteoclasts (e.g. miR-148a, miR-223, miR-21, miR-155, miR-335 and miR-29b) could contribute to osteoclast dysfunction and subsequently caused abnormal bone resorption in skeletal diseases, such as metabolic bone disease and primary/metastatic bone tumor [2–6]. The miRNA modulators, including angomir/antagomir, have been widely employed to modulate intracellular miRNAs [7,8]. However, systemic injection without any targeted delivery system would require large therapeutic dose of miRNA modulators, which may bring high risk for adverse effects due to off-target delivery, thereby bringing a major obstacle for clinical translation of those miRNA modulators [9,10]. Thus, it is highly desirable to develop an osteoclast-targeting delivery system.

Currently, a series of drug delivery systems have been designed for targeting bone microenvironment at the tissue level [11]. However, there is still lack of drug delivery system to facilitate miRNA modulators specifically targeting osteoclasts at the cellular level. It has been known that bone resorption surfaces characterized by highly crystallized hydroxyapatite are dominantly occupied by osteoclasts and osteoclast precursors [12]. It is documented that eight repeating sequences of aspartate (D-Asp₈) preferably bind to highly crystallized hydroxyapatite [12–14]. Our published data further demonstrated that D-Asp₈ could favorably bind to bone resorption surfaces [15]. Based on those findings, we postulated that D-Asp₈ could be a promising moiety for selectively approaching bone-resorption surfaces to target osteoclasts.

1,2-dioleoyl-3-trimethylammonium-propane (DOTAP)-based liposome has been approved by the U.S. Food and Drug Administration for clinical trials (NCT00059605) [15,16]. Therefore, we linked modified D-Asp₈ peptide (D-Asp₈ peptide with a C-terminal sulfhydryl residue) with DOTAP-based liposome, *i.e.* (D-Asp₈)-liposome, and subsequently encapsulated antagomir-148a, a microRNA modulator that could suppress the osteoclastogenic miR-148a to inhibit bone resorption in ovariectomized (OVX) mice [2]. Then, we examined the physical chemistry property and biological characterization of (D-Asp₈)-liposome encapsulating antagomir-148a, *i.e.* (D-Asp₈)-liposome-antagomir-148a. Further, we performed a series of *in vivo* studies to examine its tissue-/cell-selective delivery, miR-148a knockdown efficiency and therapeutic effects in OVX mice. Moreover, the targeted mechanism for osteoclast specific delivery could be explained by the interaction between D-Asp₈ and bone resorption surfaces. In addition, no detectable liver and kidney toxicity was found in mice after single/multiple dose(s) treatment of (D-Asp₈)-liposome-antagomir-148a.

2. Materials and methods

2.1. Preparation of the D-Asp₈ moiety modified liposome encapsulating antagomir-148a

The lyophilization/rehydration method was employed to encapsulate antagomir-148a in liposomes [17,18]. Firstly, the lipids of 1,2-Dioleoyl-3-Trimethylammonium-Propane (DOTAP), Dioleoylphosphatidylethanolamine

(DOPE), cholesterol (Chol), DSPE-mPEG2000 and DSPE-PEG2000-MAL at a molar ratio of 42:15:38:3:2 dissolved in chloroform were dried into a thin film and hydrated with 10 mM phosphate buffer saline (PBS, pH 7.4) pre-incubated in water bath at 50 °C to form multilamellar vesicles (MLV). The resulting MLV was then extruded in a LipoFast mini extruder (LipoFast, Avestin, Toronto, Canada) through two stacked polycarbonate membranes of 0.2 μm and 0.1 μm in stepwise manner with 5 cycles respectively to form larger unilamellar vesicles (LUV). Then, the D-Asp₈ peptide with a C-terminal sulfhydryl residue (ChinaPeptides CO., Ltd, China) was incubated with preformed liposome for 2 h at ambient temperature. The molar ratio of D-Asp₈ moiety to DSPE-PEG2000-MAL was 2:1. Subsequently, the liposome suspension was purified by size exclusion chromatography with Sepharose CL-4B column to remove the un-conjugated D-Asp₈ moiety. The quantification of cholesterol was conducted with Infinity[®] Cholesterol Liquid Stable Reagent (Thermo Electron, Melbourne, Australia) to assess the lipids concentration [19]. The liposome conjugated without D-Asp₈ moiety as control was prepared using DSPE-mPEG2000 instead of DSPE-PEG2000-MAL. The liposome suspension in 0.5 ml aliquots were mixed with 0.5 ml distilled water containing mannitol (molar ratio of mannitol-to-lipid = 5:1) and lyophilized for 48 h using freeze-dryer (Labconco, Freezone 6, USA). Finally, the above lyophilized liposomes with 15 μmol lipids were rehydrated by adding 0.5 ml DEPC-treated water containing antagomir-148a (750 μg) (Shanghai GenePharma Co., Ltd, Shanghai) and were incubated for 20 min at room temperature. The encapsulation procedure was performed immediately before use and then sterilized by passing through a 0.22 μm sterile filter.

2.2. Characteristically analysis of the D-Asp₈ moiety modified liposome by encapsulating antagomir-148a

For physical properties detection, the hydrodynamic diameters and zeta potential of (D-Asp₈)-liposome were measured by laser light scattering following their dilution with distilled water using a Delsa[®] Nano HC Particle Analyzer (Beckman Coulter, HK) at 25 °C. For encapsulation efficiency assay, the amount of antagomir-148a encapsulated inside (D-Asp₈)-liposome was assessed by the Quanti-iT[™] RiboGreen[®] RNA assay [20]. For serum stability measurement, the free antagomir-148a and antagomir-148a encapsulated in liposome or (D-Asp₈)-liposome were incubated within 50% Fetal Calf Serum, respectively. After 0.5 h, 1 h, 4 h and 24 h of incubation in the serum, the aliquots were withdrawn and the remaining antagomir-148a in the serum was purified using the miRNeasy Kit (Qiagen, Hilden, Germany) followed by separation on 2% agarose gels and visualization by ethidium bromide staining [21].

2.3. Animal handling

All the animals were housed in the Laboratory Animal House of the Institute for Advancing Translational Medicine in Bone & Joint Diseases with a temperature-controlled, 12 h light/dark cycle facility, and food and water were available *ad libitum*. The animals were acclimatized to the laboratory conditions for at least 7 days before being used in experiments. The animal study procedures were approved by the Animal Experimentation Ethics Committee of the Hong Kong Baptist University (Ref No. HASC/12-13/0032).

2.4. Tissue-selective delivery analysis of antagomir-148a in vivo

Thirty-six 3-month-old female C57BL/6 mice were ovariectomized. Then, the OVX mice were divided into four groups (n = 9 for each group): (1) free FAM-labeled antagomir-148a group, (2) *in vivo* jetPEI-FAM-labeled antagomir-148a group, (3) liposome-FAM-labeled antagomir-148a group, and (4) (D-Asp₈)-liposome-FAM-labeled antagomir-148a group. The mice were intravenously injected with free FAM-labeled antagomir-148a, or FAM-labeled antagomir-148a within *in vivo* jetPEI (a commercialized *in vivo* transfection reagent for nucleic acid), or FAM-labeled antagomir-148a within liposome alone, or the FAM-labeled antagomir-148a within (D-Asp₈)-liposome in the corresponding group, at an antagomir dose of 7.5 mg/kg at day 2 after ovariectomy. Four hours after administration, the mice were sacrificed and the major organs (heart, liver, spleen, lung, kidney, bilateral femur/tibia, and vertebra) were collected. The fluorescence signals in those organs from three mice in each group were detected using Xenogen IVIS imaging system (Xenogen Imaging Technologies, Alameda, CA). All the organs of another six mice in each group were used for quantitative study. These organs were homogenized for determining fluorescence by microplate reader [15].

2.5. Cell-selective delivery examination of antagomir-148a *in vivo*

Twenty-four 12-week old female C57BL/6 mice were ovariectomized and then divided into four groups ($n = 6$ for each group): (1) free FAM-labeled antagomir-148a group, (2) *in vivo* jetPEI-FAM-labeled antagomir-148a group, (3) liposome-FAM-labeled antagomir-148a group and (4) (D-Asp₈)-liposome-FAM-labeled antagomir-148a group. The mice were intravenously injected with free FAM-labeled antagomir-148a, or FAM-labeled antagomir-148a with *in vivo* jetPEI, or FAM-labeled antagomir-148a within liposome alone, or the FAM-labeled antagomir-148a within (D-Asp₈)-liposome in the corresponding group, at an antagomir dose of 7.5 mg/kg at day 2 after ovariectomy, and sacrificed 4 h after the administration. The tibiae were dissected and decalcified for immunohistochemistry analysis. For immunohistochemistry, the osteoclast-like cells were detected by anti-osteoclast-associated receptor (OSCAR) antibodies [22,23]. Then, the co-localization of FAM-labeled antagomir-148a with OSCAR⁺ cells was examined. On the other hand, another 12 age-matched female mice were ovariectomized and treated with rhodamine B-D-Asp₈ or unconjugated rhodamine B at day 1 after ovariectomy, respectively ($n = 6$ for each treatment group). Calcein green was simultaneously injected to these mice intraperitoneally to label bone formation. All the mice were then sacrificed at day 3 after ovariectomy. The femora were dissected after sacrifice and subsequently subjected to histomorphometric analysis and tartrate resistant acid phosphatase (TRAP) staining. Moreover, another 12 age-matched female mice were ovariectomized and pretreated with D-Asp₈ or PBS at day 2 after ovariectomy, ($n = 6$ for each pretreatment group). Thereafter, all the mice were administered with (D-Asp₈)-liposome-FAM-labeled antagomir-148a 24 h after the pretreatment. All the mice were sacrificed at day 3 after ovariectomy. The tibiae were harvested for immunohistochemistry analysis as described above.

2.6. Analysis of the dose–response pattern and persistence of miR-148a knockdown *in vivo*

To determine the dose–response pattern during *in vivo* administration, one hundred and sixty eight 3-month-old female C57BL/6 mice were ovariectomized and divided into four groups and subjected to antagomir-148a formulations dissolved in 500 μ l RNase/DNase-free PBS at a dose of 2, 4, 6, 8, 10, 15 or 20 mg/kg ($n = 6$ for each dose) via tail vein injection at day 2 after ovariectomy: (1) free antagomir-148a, (2) *in vivo* jetPEI-antagomir-148a, (3) liposome-antagomir-148a and (4) (D-Asp₈)-liposome-antagomir-148a ($n = 42$ for each group). Another 6 OVX mice injected with 500 μ l RNase/DNase-free PBS served as baseline. Two days after administration, all mice were sacrificed, and bone marrow cells were collected from the bilateral femora. Osteoclasts were sorted from bone marrow cells by FACS using antibody to OSCAR. The miR-148a expression in OSCAR⁺ cells was quantified by real-time PCR analysis, and the expression value was normalized to RNA polymerase III promoter (U6) expression. To determine the knockdown persistence of antagomir-148a *in vivo*, two hundred and forty 3-month-old female C57BL/6 mice were ovariectomized and divided into four groups: free antagomir-148a, *in vivo* jetPEI-antagomir-148a, liposome-antagomir-148a, and (D-Asp₈)-liposome-antagomir-148a ($n = 60$ for each group). All mice in each group were injected with different antagomir-148a formulations dissolved in 500 μ l RNase/DNase-free PBS at the optimal dose determined by the above dose–response experiments at day 2 after ovariectomy. Another 6 mice injected with 500 μ l RNase/DNase-free PBS served as baseline. At 1, 2, 4, 6, 8, 10, 12, 14, 16 and 18 days after treatment, the mice were sacrificed ($n = 6$ for each time point), and their bone marrow cells were collected from the bilateral femora. Osteoclasts were sorted from bone marrow cells by FACS using antibody to OSCAR. The miR-148a expression in OSCAR⁺ cells at each time point was quantified by real-time PCR analysis.

2.7. Cell-specific knockdown efficiency assay of miR-148a *in vivo*

Ninety-six 3-month-old female C57BL/6 mice were ovariectomized. Then, half of the OVX mice were intravenously administered with free antagomir-148a free antagomir-148a, *in vivo* jetPEI-antagomir-148a group, liposome-antagomir-148a or (D-Asp₈)-liposome-antagomir-148a ($n = 12$ in each treatment group) at day 2 after ovariectomy. The remaining OVX mice were subjected into four non-sense antagomir (NC) groups with non-sense antagomir substituting for antagomir-148a in the above corresponding treatment groups. The mice in each group were sacrificed at 24 and 48 h after administration ($n = 6$ per time point in each treatment group), respectively. The bone marrow cells were isolated for sorting the OSCAR⁺ and OSCAR⁻ cells by FACS as described above. The expression of miR-148a and the mRNA expression of RANK, TRAP and NFATc1 in the OSCAR⁺ and OSCAR⁻ cells were all measured by real-time PCR. Furthermore, another forty eight 3-month-old female C57BL/6 mice were ovariectomized. The OVX mice were then intravenously pretreated with D-Asp₈ or PBS ($n = 24$ for each treatment) at day 1 after ovariectomy. Then, half of the mice were administered with (D-Asp₈)-liposome-antagomir-148a and the other half of the mice were treated with non-sense antagomir at 24 h after the pretreatment. Then the mice in each group were sacrificed 24 and 48 h later ($n = 6$ for per time point in each treatment group), respectively. The bone marrow cells were isolated for sorting the OSCAR⁺ and OSCAR⁻ cells by FACS as described above. The expression of miR-148a and the mRNA expression of RANK, TRAP and NFATc1 in the OSCAR⁺ and OSCAR⁻ cells were measured by real-time PCR.

2.8. Examination of liver and kidney toxicity after single and multiple dose(s) of (D-Asp₈)-liposome-antagomir-148a

To determine the liver and kidney toxicity after a single intravenous dose of (D-Asp₈)-liposome-antagomir-148a, thirty 3-month-old healthy female C57BL/6 mice were subjected to (D-Asp₈)-liposome-antagomir-148a dissolved in 500 μ l RNase/DNase-free PBS at an antagomir-148a dose of 0, 6, 8, 10 or 15 mg/kg ($n = 6$ for each dose) via tail vein injection. 72 h after administration, biochemical parameters, *i.e.* ALT (alanine aminotransferase); AST (aspartate aminotransferase) and BUN (blood urea nitrogen), were examined. To determine the liver and kidney toxicity after multiple intravenous injections of (D-Asp₈)-liposome-antagomir-148a, another twelve 3-month-old healthy female C57BL/6 mice received periodic intravenous doses of (D-Asp₈)-liposome-antagomir-148a dissolved in 500 μ l RNase/DNase-free PBS at an antagomir-148a dose of 0 or 8 mg/kg. The same biochemical parameters were examined.

2.9. Therapeutic effect evaluation of antagomir-148a delivered by (D-Asp₈)-liposome on OVX mice

Totally, sixty-six female C57BL/6 mice were ovariectomized ($n = 54$) or sham-operated ($n = 12$) at 3 months of age, and they were subsequently divided into OVX baseline group, OVX + PBS group (control), OVX + free antagomir-148a group, OVX + *in vivo* jetPEI-antagomir-148a group, OVX + liposome-antagomir-148a group, OVX + (D-Asp₈)-liposome-antagomir-148a group, OVX + D-Asp₈ group, OVX + D-Asp₈ + (D-Asp₈)-liposome-antagomir-148a group, OVX + PBS + (D-Asp₈)-liposome-antagomir-148a group, Sham baseline group and Sham + PBS group ($n = 6$ for each group) according to treatment. Increased osteoclastic bone resorption is dominant at the early stage after ovariectomy, providing an optimal observation window to evaluate our osteoclast-targeted delivery system. Thus, we started treatment at 2 days after ovariectomy procedure. Briefly, the mice in the OVX baseline group or Sham baseline group were sacrificed at day 1 after ovariectomy or sham-operation as baseline before treatment initiation. At day 2 after ovariectomy, the mice in OVX + free antagomir-148a, OVX + *in vivo* jetPEI-antagomir-148a, OVX + liposome-antagomir-148a, OVX + (D-Asp₈)-liposome-antagomir-148a and OVX + PBS groups began to receive six periodic intravenous injections of free antagomir-148a, *in vivo* jetPEI-antagomir-148a, liposome-antagomir-148a, (D-Asp₈)-liposome-antagomir-148a and PBS every week, respectively, at an antagomir-148a dose of 8 mg/kg. On the other hand, the mice in the OVX + D-Asp₈ group were pretreated with D-Asp₈ at day 1 after ovariectomy and received intravenous injections of PBS 24 h after the pretreatment. The mice in the OVX + D-Asp₈ + (D-Asp₈)-liposome-antagomir-148a group and OVX + PBS + (D-Asp₈)-liposome-antagomir-148a group were pretreated with D-Asp₈ and PBS at day 1 after ovariectomy, respectively, and were administered with (D-Asp₈)-liposome-antagomir-148a 24 h after the pretreatment, at an antagomir-148a dose of 8 mg/kg. The regimens in the above three groups repeated six times at the interval of 1 week. The mice in the Sham + PBS group were intravenously treated with PBS for six weeks. All the mice in each treatment group were sacrificed at six weeks after the first treatment. After sacrifice, the 5th lumbar bodies (LV5) were collected and sequentially subjected to micro-CT measurement and bone histomorphometry. The tibiae were harvested for total RNA extraction followed by reverse transcription PCR and real-time PCR analysis to determine the mRNA expression of TRAP (osteoclast marker gene) [2]. The serum were collected for ELISA to examine the level of CTX-I (serum bone resorption marker) [24].

2.10. HPLC analysis for conjugation of D-Asp₈ moiety to liposome surfaces

Free D-Asp₈-SH equivalent to 1 mg/ml D-Asp₈-SH before and after the conjugation reaction were analyzed by HPLC to ascertain its status. A Kromasil[®] C18-column (4.6 \times 250 mm, Amsterdam, Netherlands) was used with a mobile phase consisting of 0.1% trifluoroacetic acid in water (solution A) and 0.1% trifluoroacetic acid in acetonitrile (solution B). The solution gradient was set from 10% to 30% B in 20 min, and subsequently back to 10% solution B over 10 min. The detection wavelength was 220.8 nm, the flow rate was 1 ml/min, and the injection volume was 20 μ l [25].

2.11. Biophotonic imaging analysis

Fluorescence imaging for FAM labeled antagomir-148a distribution in these organs was performed using an IVIS[®] 200 imaging system. Excitation ($\lambda_{ex} = 445\text{--}490$ nm) and Emission ($\lambda_{em} = 515\text{--}575$ nm) filters were used. Identical illumination settings, including exposure time (5 s), binning factor (4), f-stop (2) and fields of view (15 cm for width and length, respectively), were used for all imaging acquisition. Fluorescent and photographic images were acquired and overlaid. The pseudo color image represents the spatial distribution of photon counts within the bone. Background fluorescence taken under background filter (410–440 nm) was subtracted prior to analysis [19,26].

2.12. Microplate reader analysis

The bone tissues, including bilateral femur/tibia and vertebra, were firstly crushed into pieces after they have frozen with liquid nitrogen and then

homogenized [27]. The excised tissues except femur and tibia were directly homogenized in lysis buffer (0.1% sodium dodecyl sulfate in phosphate-buffered saline, 1000 μ l for livers and 300 μ l for others) and incubated at 65 °C for 10 min. After centrifugation at 14,000 rpm for 15 min, 150 μ l of supernatant was collected and transferred to a black 96-well plate. The fluorescence intensity of the organ samples were measured by a microplate reader (Bioscan, Washington, DC) at λ_{ex} : 485 nm and λ_{em} : 535 nm. FAM-labeled antagomir-148a concentration in each sample was calculated from a standard curve by spiking known amounts of FAM-labeled antagomir-148a or FAM-labeled antagomir-148a encapsulated by carriers in supernatant from tissues of un-injected animals [15]. The accumulation of FAM-labeled antagomir-148a in each tissue was expressed by the amount of FAM-labeled antagomir-148a in each tissue divided by the injected antagomir-148a dose.

2.13. Immunohistochemistry

Bilateral femur and tibia were dissected at 4 h after administration with free FAM-labeled antagomir-148a and FAM-labeled antagomir-148a delivered by *in vivo* jetPEI, liposome or (D-Asp₈)-liposome, then fixed with 4% buffered formalin and embedded with optimal cutting temperature compound (O.C.T.) after decalcification with 10% EDTA. The frozen frontal section (5 μ m thickness) from each group was cut in a freezing cryostat at –20 °C. The sections were air dried at room temperature, fixed in ice-cold acetone for 10 min, permeabilized with 0.1% Triton X-100 at room temperature for 20 min, and blocked in 5% donkey serum in PBS. The sections were then incubated overnight at 4 °C with goat polyclonal OSCAR (1:50 dilution; Santa Cruz Biotechnology, Inc.). Following three washes in PBS, the sections were incubated with Alexa Fluor 555-conjugated donkey anti-goat IgG (1:300 dilution; Invitrogen) for 1 h. Negative control experiments were done by omitting the primary antibodies. The sections were mounted with the medium containing DAPI (Vector Laboratories). The sections were examined under a fluorescence microscope (Q500MC, Leica image analysis system) [15,28].

2.14. Fluorescence active cell sorting

The bone marrow cells were collected from the mice femur and tibia. The goat polyclonal antibody to mouse OSCAR (Santa Cruz Biotechnology, USA) was used for fluorescence active cell sorting (FACS). After washed by PBS/1% BSA, the cells were directly incubated with antibody to OSCAR (1:4) and then stained with donkey anti-goat IgG-FITC (1:100, Santa Cruz Biotechnology, USA). After that, stained cell populations were used for FACS. The obtained selected OSCAR⁺ cell population and start cell population were used for total RNA extraction and real-time PCR [15,28].

2.15. Total RNA extraction, reverse transcription and quantitative real-time PCR

An RNeasy Mini Kit (Qiagen, Cat. No. 74106) was used to extract total RNA from cells using the manufacturer's protocol. Total RNA was reverse transcribed into cDNA using a QuantiTect Reverse Transcription Kit according to an established protocol. The 10 μ l volume of the final quantitative real-time PCR solution contained 1 μ l of diluted cDNA product, 5 μ l of 2 \times Power SYBR[®] Green PCR Master Mix (Applied Biosystems, Foster City, CA, USA), 0.5 μ l each of forward and reverse primers and 3 μ l of nuclease-free water. The forward and reverse primers for miR-148a, RANK, TRAP and NFATc1 were used as previously described (2). The amplification conditions were as follows: 50 °C for 2 min, 95 °C for 10 min, 40 cycles of 95 °C for 15 s and 60 °C for 1 min. The emitted fluorescence signal was collected by an ABI PRISM[®] 7900HT Sequence Detection System, and the signal was converted into numerical values by SDS 2.1 software (Applied Biosystems) [28,29].

2.16. Assays of biochemical parameters and urine bone resorption marker levels

A series of clinical biochemical parameters (ALT, AST and BUN) were analyzed using a clinical chemistry analyzer (Cruinn Diagnostics Ltd., Ireland). The serum bone resorption marker CTX-1 was measured by ELISA kits for mouse cross linked C-Telopeptide of Type 1 Collagen (Uscn Life Science Inc., Wuhan, China) following the manufacturer's protocol.

2.17. Micro-CT analysis

The LV5 was dissected and scanned by micro-CT system (viva CT40, SCANCO MEDICAL, Switzerland) and analyzed. Briefly, a total of 350 slices with a voxel size of 15 μ m were scanned at the entire region of secondary spongiosa between proximal and distal aspects from the vertebral body. The whole trabecular bone was isolated for three-dimension reconstruction (Sigma = 1.2, Supports = 2 and Threshold = 200) to calculate the following parameters: bone mineral density (BMD) and relative bone volume (BV/TV) [28,30].

2.18. Bone histomorphometric analysis

For bone histomorphometric analysis, the bone specimen (LV5 or tibiae in the corresponding study) of each mice was dehydrated in graded concentrations of ethanol and embedded without decalcification in modified methyl methacrylate. Frontal sections of trabecular bone at a thickness of 10 μ m were obtained from the distal femur with an EXAKT Cut/Grinding System (EXAKT Technologies, Inc. Germany). Fluorescence micrographs for the Rhodamin-B and calcein labeling in the

bone sections were captured by a fluorescence microscope (Leica image analysis system). Thereafter, the above bone sections underwent standard TRAP staining followed by bone histomorphometric analyses of the bone resorption-relative parameters, *i.e.* osteoclast surface (Oc.S/BS) and osteoclast number (Oc.N/B.Pm), were performed using professional image analysis software (ImageJ, NIH, USA and BIOQUANT OSTEO analysis software, Version 13.2.6, Nashville, TN, USA) and the above microscope under bright field [28,30]. Briefly, 25 systematically random fields of view were taken in each section under the 20 \times objective magnification within the trabecular compartment. Histomorphometric data are reported according to the standardized nomenclature [31].

2.19. Statistical analysis

All the variables were expressed as mean \pm standard deviation. One-way ANOVA with LSD's *post hoc* test was performed to determine inter-group differences in the study variables. $P < 0.05$ was considered statistically significant. All the statistical data in this project was analyzed by a contract service from Bioinformedicine (San Diego, CA, USA, <http://www.bioinformedicine.com/index.php>).

3. Results

3.1. Preparation of (D-Asp₈)-liposome-antagomir-148a

A schematic diagram illustrated the detailed preparative procedures of (D-Asp₈)-liposome-antagomir-148a (Supplementary Fig. 1a). Briefly, multilamellar vesicles (MLV) were prepared and extruded to form large unilamellar vesicles (LUV). Then, the D-Asp₈ peptide with a C-terminal sulfhydryl residue (D-Asp₈-SH) was conjugated to the DOTAP-based liposomes to form (D-Asp₈)-liposome. The HPLC data showed that the peak of free D-Asp₈-SH at concentration of 1 mg/ml eluted with a retention time of 8.8 min before the conjugation reaction, whereas the peak area decreased after the conjugation reaction (Supplementary Fig. 1b), indicating that D-Asp₈-SH was linked to the DOTAP-based liposomes. After purification, (D-Asp₈)-liposome was lyophilized and rehydrated by the solution of antagomir-148a in order to encapsulate it inside liposome according to the standard methods described in the 'Materials and methods'.

3.2. Characterization of (D-Asp₈)-liposome-antagomir-148a

The data from laser light scattering measurement showed that the average hydrodynamic diameter of (D-Asp₈)-liposome-antagomir-148a was 150 nm (Fig. 1a) and the zeta potential of (D-Asp₈)-liposome-antagomir-148a was about –10 mV. Meanwhile, the data from Quant-iT[™] RiboGreen[®] RNA assay demonstrated that the encapsulation efficiency of the (D-Asp₈)-liposome was about 80.15% for antagomir-148a. Furthermore, the agarose gel electrophoresis analysis showed that the band of antagomir-148a was still detectable 24 h later after incubation of (D-Asp₈)-liposome-antagomir-148a (Fig. 1b) or liposome-antagomir-148a (data not shown) with serum, whereas it could not be detected 1 h later after incubation of free antagomir-148a with serum (Fig. 1b).

3.3. Tissue-selective delivery of antagomir-148a encapsulated by (D-Asp₈)-liposome *in vivo*

The biophotonic imaging techniques were used to examine the tissue distribution of free FAM-labeled antagomir-148a, FAM-labeled antagomir-148a delivered by *in vivo* jetPEI, FAM-labeled antagomir-148a delivered by liposome and FAM-labeled antagomir-148a delivered by (D-Asp₈)-liposome, respectively, in 3-month-old female OVX mice. The data showed that the fluorescence signals of FAM-labeled antagomir-148a in bone tissues were the strongest in the mice injected with (D-Asp₈)-liposome-FAM-labeled antagomir-148a among all the groups. However, the fluorescence signals of FAM-labeled antagomir-148a in the livers and kidneys were lower in the mice treated with (D-Asp₈)-

liposome-FAM-labeled antagomir-148a than those in the mice treated with free FAM-labeled antagomir-148a or FAM-labeled antagomir-148a delivered either by *in vivo* jetPEI or liposome, respectively. The fluorescence signals of FAM-labeled antagomir-148a were barely detected in the hearts, spleens and lungs of the mice from all the groups (Fig. 2a). Furthermore, the quantitative data from the fluorescence assay by microplate readers were also in consistent with the findings from the biophotonic imaging analysis (Fig. 2b).

3.4. Cell-selective delivery of antagomir-148a encapsulated by (D-Asp₈)-liposome *in vivo*

Immunofluorescence analysis was performed to determine the cellular distribution of free FAM-labeled antagomir-148a, FAM-labeled antagomir-148a delivered by *in vivo* jetPEI, FAM-labeled antagomir-148a delivered by liposome and FAM-labeled antagomir-148a delivered by (D-Asp₈)-liposome, respectively, in 3-month-old OVX mice after treatment. The cryosections of the distal femur from the above mice were immunostained with antibody to osteoclast-associated receptor (OSCAR), a surface marker specifically expressed in pre-osteoclasts and mature osteoclasts [22,23]. The fluorescence micrographs showed numerous instances for co-localization of the FAM-labeled antagomir-148a with OSCAR-positive (OSCAR+) cells in the (D-Asp₈)-liposome-FAM-labeled antagomir-148a group, whereas few instances of such co-staining were found in the other groups (Fig. 3a). To examine whether D-Asp₈ could preferentially bind to bone resorption surfaces to facilitate antagomir-148a selectively targeting osteoclasts, another two groups of 3-month-old OVX mice were treated with rhodamine B-conjugated D-Asp₈ and unconjugated rhodamine B at day 1 after ovariectomy, respectively. Calcein green was also simultaneously injected to these mice intraperitoneally to label bone formation. All the mice were then sacrificed at day 3 after ovariectomy. As shown in the fluorescence micrographs of the undecalcified trabecular bone sections, rhodamine B labeling was found at the eroded surfaces opposite to the calcein green-labeled bone formation surfaces in the mice co-treated with rhodamine B-conjugated D-Asp₈ and calcein green (Fig. 3b). The tartrate-resistant acid phosphatase (TRAP) staining data further showed that the above rhodamine B-labeled bone surfaces were occupied by osteoclasts (Fig. 3b). However, no rhodamine B labeling was observed in the mice co-treated with unconjugated rhodamine B and calcein green (Fig. 3b). In addition, another two groups of 3-month-old OVX mice were pretreated with D-Asp₈ and PBS at day 1 after ovariectomy, respectively. Thereafter, they were administrated with (D-Asp₈)-liposome-FAM-labeled antagomir-148a at day 2 after ovariectomy

and sacrificed 24 h later. The immunofluorescence data showed significantly fewer instances for co-localization of FAM-labeled antagomir-148a and OSCAR+ cells at the cryosection of distal femora from the mice pretreated with D-Asp₈ when compared to those pretreated with PBS (Fig. 3c).

3.5. Dose-response pattern and persistence of miR-148a knockdown by antagomir-148a delivered by (D-Asp₈)-liposome *in vivo*

The dose–response pattern and persistence of miR-148a knockdown in OSCAR+ cells by free antagomir-148a or antagomir-148a delivered by *in vivo* jetPEI, liposome or (D-Asp₈)-liposome were determined by FACS in combination with real-time PCR analysis. The knockdown efficiency of antagomir-148a increased in a dose dependent manner at the dose ranging from 2 mg/kg to 8 mg/kg and **almost 80% knockdown efficiency was achieved at a dose of 8 mg/kg in the (D-Asp₈)-liposome-antagomir-148a group**. However, no obvious miR-148a knockdown (over 50%) was achieved at the same dose in the free antagomir-148a, *in vivo* jetPEI-antagomir-148a or liposome-antagomir-148a group (Fig. 4a). After a single injection of (D-Asp₈)-liposome-antagomir-148a at a dose of 8 mg/kg, almost complete miR-148a knockdown was found at 48 h, and over 50% miR-148a knockdown was maintained for 8 days. However, no obvious miR-148a knockdown (over 50%) was observed at any time point after the treatment of the same dose in the free antagomir-148a, *in vivo* jetPEI-antagomir-148a or liposome-antagomir-148a group (Fig. 4b).

3.6. Cell-specific knockdown efficiency of miR-148a by antagomir-148a delivered by (D-Asp₈)-liposome *in vivo*

Fluorescence-activated cell sorting (FACS) and real-time polymerase chain reaction (PCR) analysis were performed to examine the knockdown efficiency of antagomir-148a in bone marrow-derived OSCAR+ cells from the 3-month-old OVX mice treated with free antagomir-148a, antagomir-148a delivered by *in vivo* jetPEI, antagomir-148a delivered by liposome and antagomir-148a delivered by (D-Asp₈)-liposome, respectively. The data showed that the miR-148a knockdown efficiency in OSCAR+ cells was significantly higher than that in OSCAR-negative (OSCAR-) cells at both 24 and 48 h after treatment with (D-Asp₈)-liposome-antagomir-148a. In contrast, no significant difference in the knockdown efficiency of miR-148a was found between the OSCAR+ and OSCAR-cells after treatment with free antagomir-148a, *in vivo* jetPEI-antagomir-148a and liposome-antagomir-148a, respectively (Fig. 5a). The mRNA expression of the osteoclast-related markers (RANK, TRAP and

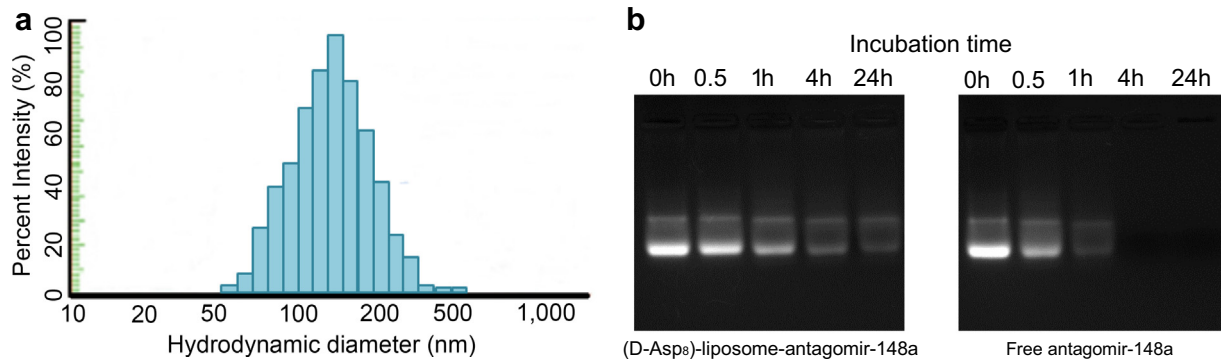


Fig. 1. Characterization of (D-Asp₈)-liposome-antagomir-148a *in vitro*. (a) The average hydrodynamic diameter of (D-Asp₈)-liposome-antagomir-148a was 150 nm. (b) The stability of the free antagomir-148a and antagomir-148a encapsulated by (D-Asp₈)-liposome were determined by agarose gel electrophoresis at the indicted time point after incubation within serum.

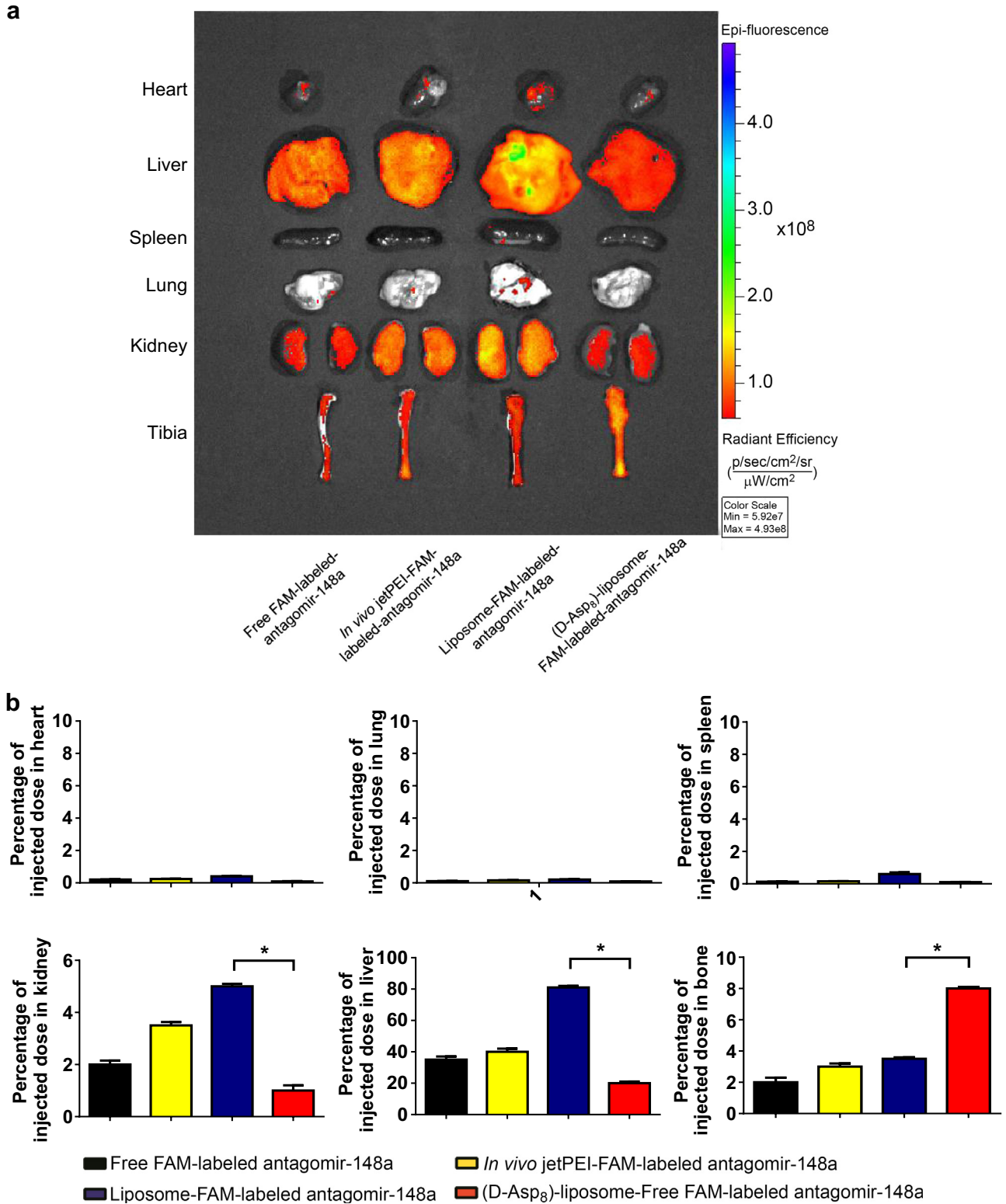


Fig. 2. Tissue-selective delivery of antagomir-148a *in vivo*. (a) Representative images for the tissue distribution of the FAM-labeled antagomir-148a (FAM-antagomir-148a) in OVX mice by a biophotonic imaging after administration of free FAM-labeled antagomir-148a, *in vivo* jetPEI-FAM-labeled antagomir-148a, liposome-FAM-labeled antagomir-148a and (D-Asp₈)-liposome-FAM-labeled antagomir-148a, respectively. The fluorescence signals was analyzed in the isolated hearts, livers, spleens, lungs, kidneys and proximal tibiae from the mice in each group. n = 3 per group. (b) Quantitative analysis by a microplate reader system for the fluorescence signal density of the FAM-labeled antagomir-148a in hearts, livers, spleens, lungs, kidneys and bone tissues after administration of free FAM-labeled antagomir-148a, *in vivo* jetPEI-FAM-labeled antagomir-148a, liposome-FAM-labeled antagomir-148a and (D-Asp₈)-liposome-FAM-labeled antagomir-148a in a separated sets of OVX mice. The bone tissues included bilateral femora and tibiae samples, as well as vertebra samples. Note: The data were presented as the mean ± s.d., n = 6 per group. *P < 0.05 for comparison with the liposome-FAM-labeled antagomir-148a group.

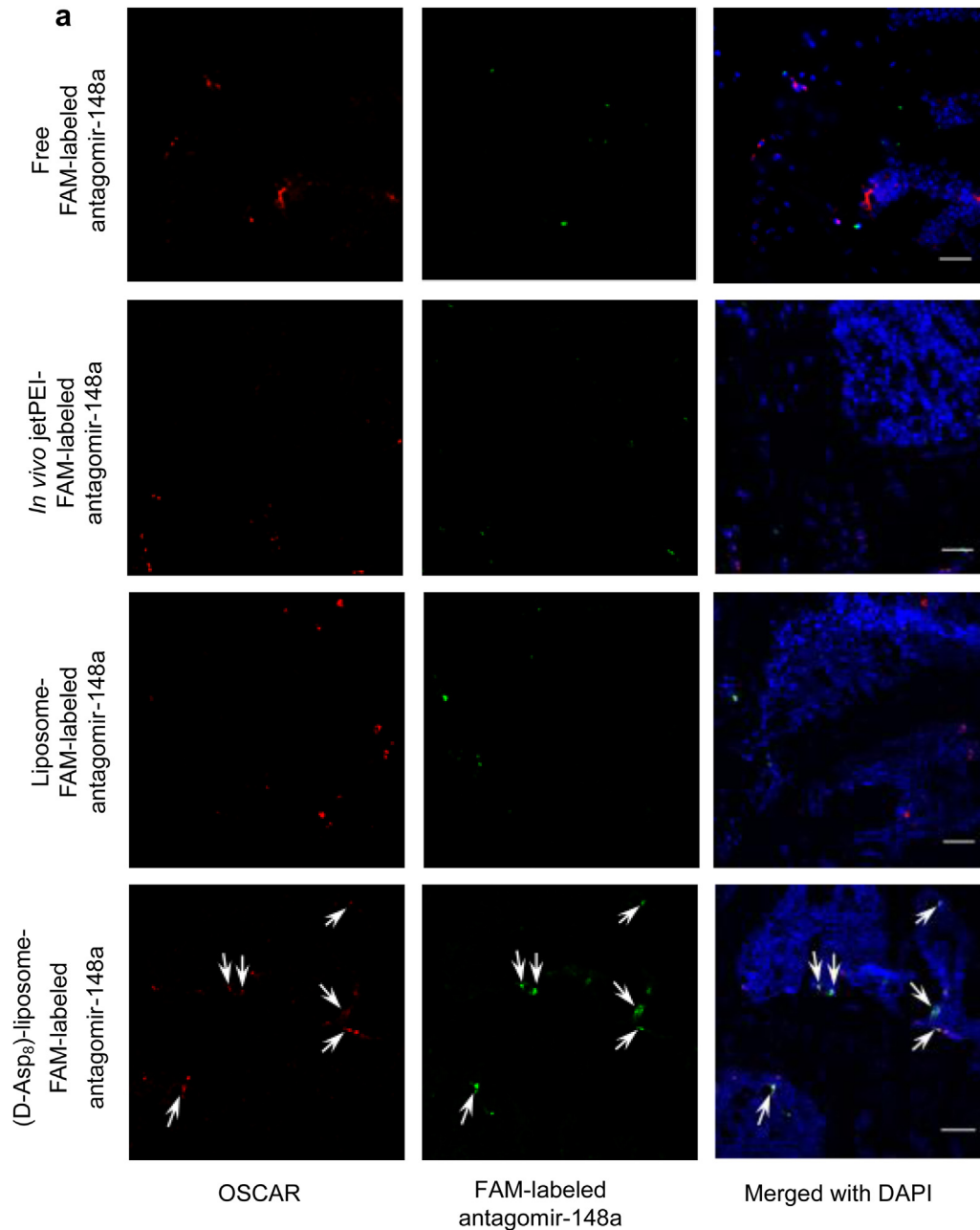


Fig. 3. Cell-selective delivery of antagomir-148a *in vivo*. (a) Representative fluorescence micrographs of the cryosections of proximal tibiae from the mice administrated with free FAM-labeled antagomir-148a, *in vivo* jetPEI-FAM-labeled antagomir-148a, liposome-FAM-labeled antagomir-148a and (D-Asp₈)-liposome-FAM-labeled antagomir-148a, respectively. Immunohistostaining was performed to detect OSCAR⁺ cells (osteoclasts; red; left column). The antagomir-148a was labeled with FAM (green; middle column). Merged images with DAPI staining showed co-localization of FAM-labeled antagomir-148a and OSCAR⁺ cells (arrows; right column). Scale bar = 20 μ m. (b) Representative fluorescence micrographs of the undecalcified bone sections from the distal femora (left three) and representative bright field micrographs of the same sections with TRAP staining (right) in the mice treated with Rhodamine B-D-Asp₈ (top panel) or unconjugated rhodamine B (bottom panel). The white arrows indicate the Rhodamine B labeling (red). The bone formation surfaces were labeled by calcein (green). The black arrows indicate the TRAP stained bone resorption surfaces which co-localized with Rhodamine B labeling. Scale bar = 50 μ m. (c) Representative fluorescence micrographs of cryosections of the proximal tibia from the mice pretreated with D-Asp₈ or PBS followed by the administration of (D-Asp₈)-liposome-FAM-labeled antagomir-148a. Immunohistostaining was performed to detect OSCAR⁺ cells (osteoclasts; red; left column). The antagomir-148a was labeled with FAM (green; middle column). Merged images with DAPI staining showed co-localization of FAM-antagomir-148a and OSCAR⁺ cells (arrows; right column). Scale bar = 20 μ m. (For interpretation of the references to colour in this figure legend, the reader is referred to the web version of this article.)

NFATc1) in OSCAR⁺ cells were remarkably down-regulated in (D-Asp₈)-liposome-antagomir-148a group but not in the other treatment groups at 48 h after treatment (Fig. 5b). Furthermore, the cell-specific knockdown of miR-148a by antagomir-148a delivered by (D-Asp₈)-liposome with or without D-Asp₈ pretreatment was examined in 3-month-old OVX mice. The data showed that, compared with the mice without D-Asp₈ pretreatment, the

significant difference in miR-148a knockdown efficiency between the OSCAR⁺ and OSCAR⁻ cells at both 24 and 48 h was undetectable in the mice with D-Asp₈ pretreatment (Fig. 5c). Similarly, the aforementioned inhibitory effect on the expression of osteoclast-related marker genes in OSCAR⁺ cells by (D-Asp₈)-liposome-antagomir-148a treatment could be prevented when the mice were pretreated with D-Asp₈ (Fig. 5d).

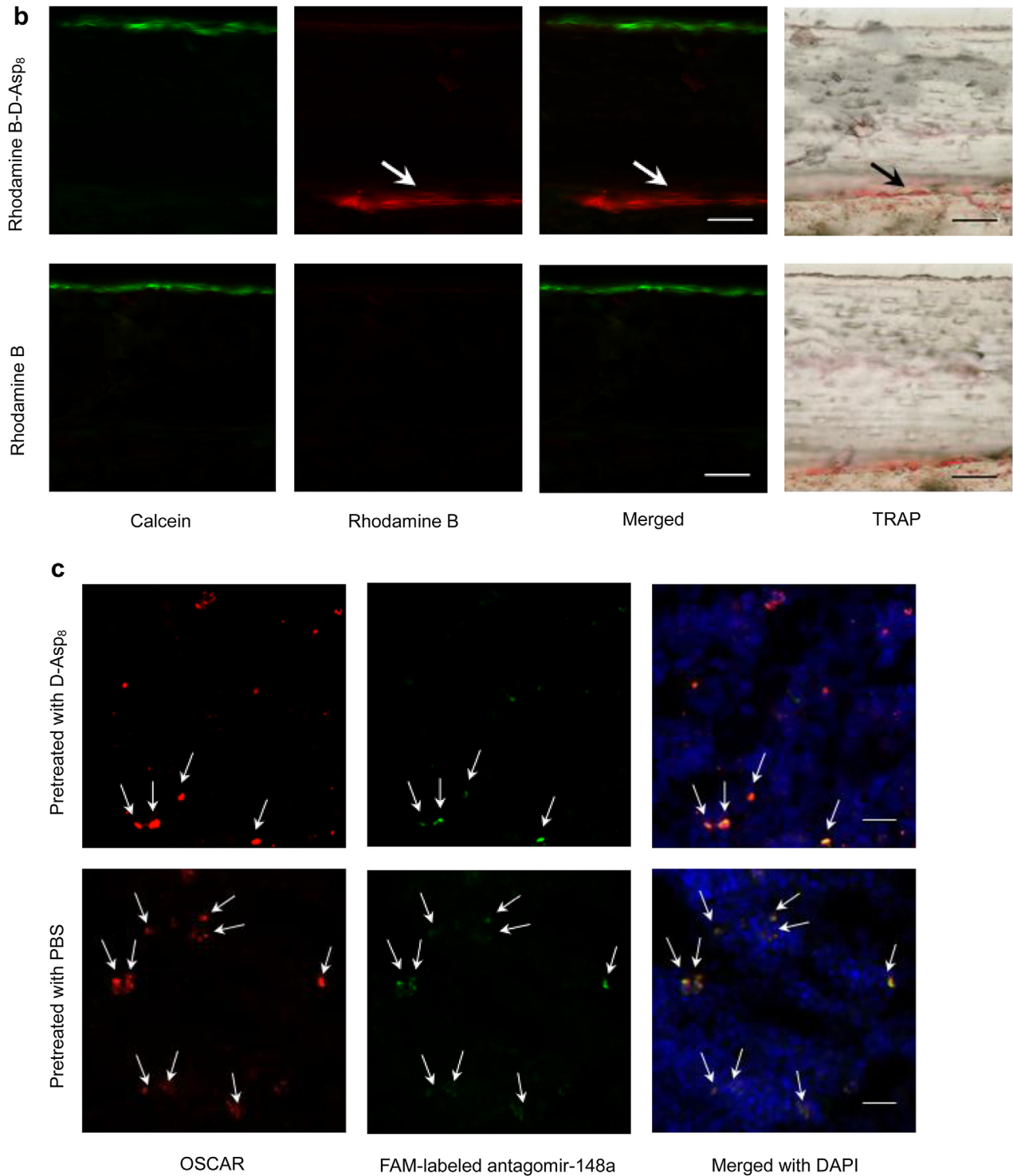


Fig. 3. (continued).

3.7. Toxicity analysis of (D-Asp₈)-liposome-antagomir-148a in healthy mice after single/multiple dose(s) treatment

To evaluate the liver and kidney toxicity of (D-Asp₈)-liposome-antagomir-148a, the changes in blood biochemical parameters of liver and kidney function were examined in 3-month-old healthy female mice after single/multiple dose(s) treatment of (D-Asp₈)-liposome-antagomir-148a. There were no statistically significant

differences in either the liver function indexes (alanine aminotransferase (ALT) and aspartate aminotransferase (AST)) or the kidney function index (blood urea nitrogen (BUN)) between the mice injected with (D-Asp₈)-liposome-antagomir-148a at a single dose ranging from 6 to 15 mg/kg and the mice injected with phosphate-buffered saline (PBS). In addition, no obvious differences in the above biochemical parameters were found between the mice treated with six periodic injections of (D-Asp₈)-liposome-

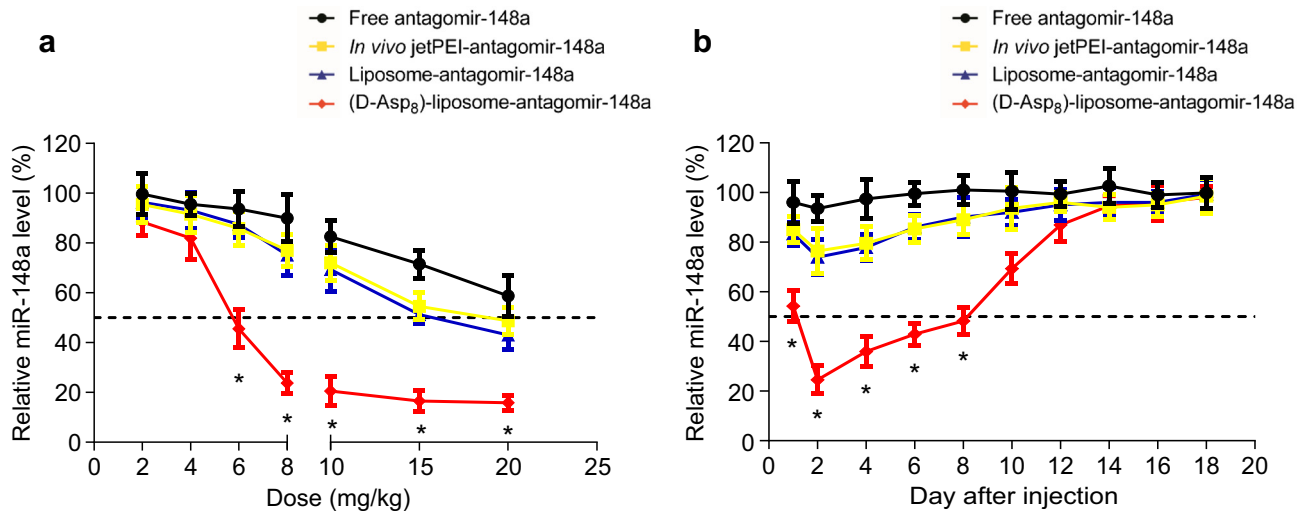


Fig. 4. Dose-response pattern and persistence of miR-148a knockdown *in vivo*. (a) Dose-dependent antagomir-148a knockdown determined by real-time PCR (RT-PCR) and normalized to the baseline after tail vein injection of free antagomir-148a, *in vivo* jetPEI-antagomir-148a, liposome-antagomir-148a or (D-Asp₈)-liposome-antagomir-148a at a single antagomir-148a dose ranging from 2 to 20 mg/kg. (b) Persistence of miR-148a knockdown examined by RT-PCR and normalized to the baseline after a single injection of free antagomir-148a, *in vivo* jetPEI-antagomir-148a, liposome-antagomir-148a, or (D-Asp₈)-liposome-antagomir-148a at the antagomir-148a dose of 8 mg/kg. Note: The miR-148a expression levels in each group were normalized by the U6 expression level. The data were presented as the mean \pm s.d., $n = 6$ per dose or per time point in each group. * $P < 0.05$ for a comparison of (D-Asp₈)-liposome-antagomir-148a group with free antagomir-148a or *in vivo* jetPEI-antagomir-148a or liposome-antagomir-148a group.

antagomir-148a at the dose of 8 mg/kg and the mice treated with six periodic injections of PBS at the same interval of one week (Supplementary Table).

3.8. Therapeutic effects of antagomir-148a delivered by (D-Asp₈)-liposome in OVX mice

Micro computed tomography (microCT), bone histomorphometry, ELISA and real time PCR analysis were all employed to measure the bone mass, trabecular structure and bone resorption in the OVX mice after administration with PBS, free antagomir-148a, antagomir-148a delivered by *in vivo* jetPEI, antagomir-148a delivered by liposome and antagomir-148a delivered by (D-Asp₈)-liposome, respectively. Another group of mice were sacrificed at day 1 after ovariectomy as baseline before treatment. As shown by the micro-CT data, no substantial differences in the bone mineral density (BMD) and relative bone volume (BV/TV) were found between the Sham baseline and Sham + PBS group (Supplementary Fig. 2). However, the BMD and BV/TV were dramatically decreased from the baseline level in the OVX + PBS group six weeks after ovariectomy, whereas the above decreases were remarkably attenuated in the (D-Asp₈)-liposome-antagomir-148a group. No statistically significant attenuation of the decreases in BMD and BV/TV after ovariectomy were found in the free antagomir-148a, *in vivo* jetPEI-antagomir-148a and liposome-antagomir-148a groups. Moreover, both the above two micro-CT parameters in the (D-Asp₈)-liposome-antagomir-148a group were remarkably higher than those in the other treatment groups (Fig. 6a). As shown by the reconstructed micro-CT images, better organized trabecular micro-architecture was found in the (D-Asp₈)-liposome-antagomir-148a group when compared to those in the other treatment groups (Fig. 6b). Furthermore, the bone histomorphometric data showed that the N.Oc/BPm (osteoclast number, mm⁻¹) and Oc.S/BS (osteoclast surface, %) were both significantly increased from the baseline level in the OVX + PBS group six weeks after ovariectomy. However, the above increases were dramatically attenuated in the (D-Asp₈)-liposome-antagomir-148a group. Similarly, no statistically significant attenuation of the increases in N.Oc/BPm and Oc.S/BS after ovariectomy were observed in the free antagomir-148a, *in vivo* jetPEI-antagomir-148a and liposome-

antagomir-148a groups. In addition, both the two histomorphometric parameters in the (D-Asp₈)-liposome-antagomir-148a group were significantly lower than those in the other treatment groups (Fig. 6c). Moreover, the intra-osseous TRAP (Tartrate-resistant acid phosphatase) mRNA expression and serum CTX-I (C-Terminal Telopeptides Type I Collagen) level were both remarkably increased from the baseline level in the OVX + PBS group six weeks after ovariectomy. However, the above increases were notably attenuated in the (D-Asp₈)-liposome-antagomir-148a group. Similarly, no statistically significant attenuation of the increases in the above two variables after ovariectomy were found in the free antagomir-148a, *in vivo* jetPEI-antagomir-148a and liposome-antagomir-148a groups (Fig. 6d). On the other hand, the influence of D-Asp₈ pretreatment on the therapeutic effect of antagomir-148a delivered by (D-Asp₈)-liposome was also evaluated. Impressively, the above attenuation effects by (D-Asp₈)-liposome-antagomir-148a treatment were not found in the group with D-Asp₈ pretreatment before the administration of (D-Asp₈)-liposome-antagomir-148a (Fig. 6).

4. Discussion

To date, there is lack of delivery system to facilitate miRNA modulators specifically targeting osteoclasts *in vivo*. In this study, we generated a delivery system, *i.e.* (D-Asp₈)-liposome, to specifically approach bone resorption surfaces to achieve delivery of miRNA modulators into osteoclasts. It would potentially facilitate the clinical translation of miRNA modulators in treating skeletal diseases caused by dysfunctional osteoclasts.

In our chemical conjugation study, the free D-Asp₈-SH was successfully conjugated to the maleimide group on the surfaces of liposome, as indicated by the diminution of free D-Asp₈-SH after the conjugation reaction. Moreover, the serum stability data suggested that (D-Asp₈)-liposome could protect antagomir-148a from degradation by endogenous nucleases in serum, as indicated by the agarose gel electrophoresis analysis showing significantly longer period for the detectable antagomir-148a in (D-Asp₈)-liposome-antagomir-148a group when compared to that in free antagomir-148a group. In addition, no difference was found in serum stability data between (D-Asp₈)-liposome-antagomir-148 group and liposome-antagomir-148

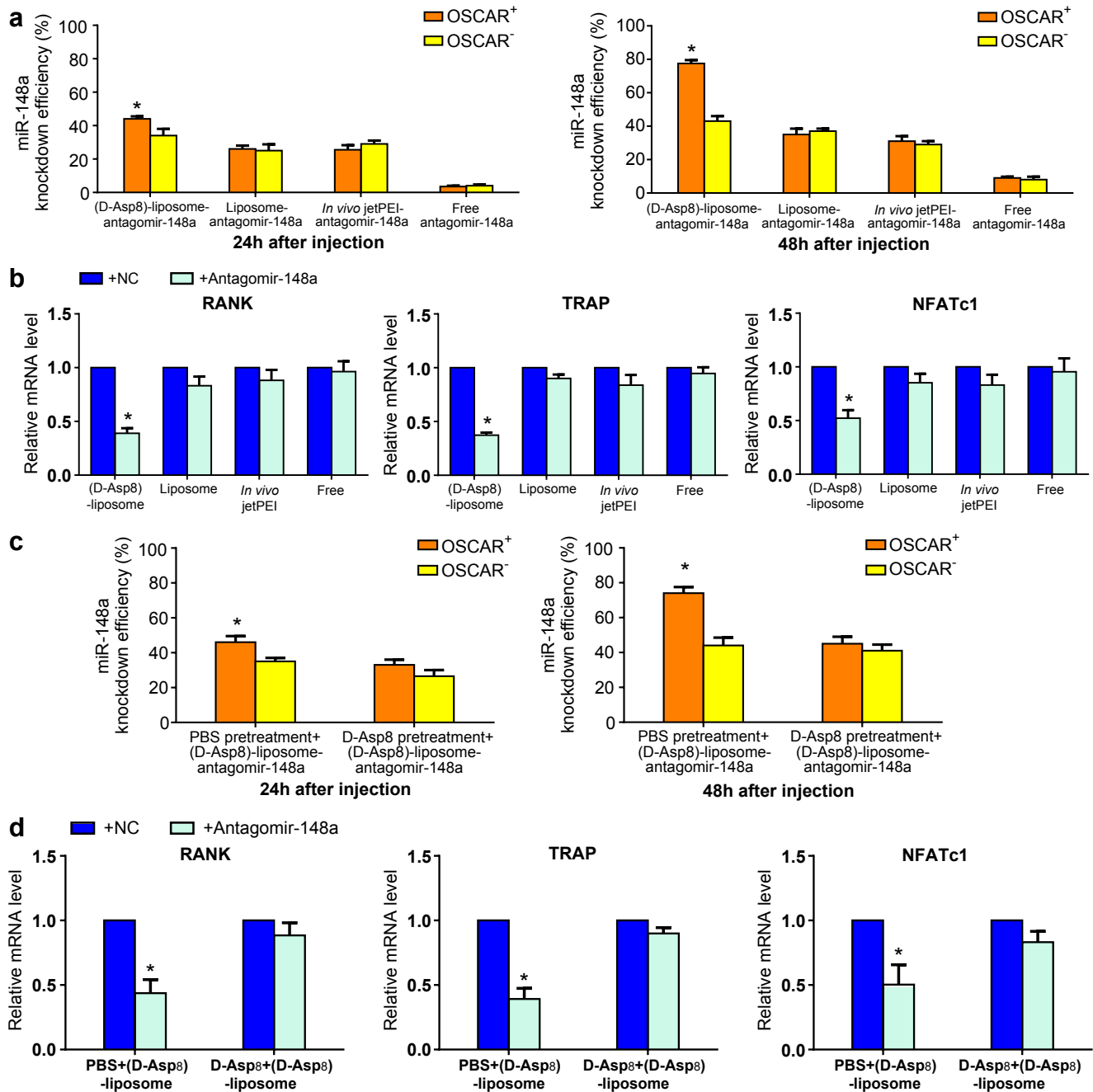


Fig. 5. Cell-specific knockdown efficiency of miR-148a *in vivo*. (a) Real-time PCR (RT-PCR) analysis for the miR-148a knockdown efficiency in OSCAR⁺ and OSCAR⁻ cells sorted from bone marrows (BMs) by fluorescence-activated cell sorting (FACS) from the ovariectomized (OVX) mice administrated with free antagomir-148a, *in vivo* jetPEI-antagomir-148a, liposome-antagomir-148a or (D-Asp₈)-liposome-antagomir-148a at 24 h and 48 h after administration. (b) RT-PCR analysis for the mRNA expression of RANK, TRAP and NFATc1 in the OSCAR⁺ cells sorted from BMs by FACS from the OVX mice administrated with free antagomir-148a, *in vivo* jetPEI-antagomir-148a, liposome-antagomir-148a or (D-Asp₈)-liposome-antagomir-148a at 48 h after administration. (c) RT-PCR analysis for the miR-148a knockdown efficiency in OSCAR⁺ and OSCAR⁻ cells sorted from BMs by FACS from the OVX mice pretreated with D-Asp₈ or PBS followed by the administration of (D-Asp₈)-liposome-antagomir-148a at 24 h and 48 h after administration. (d) RT-PCR analysis for the mRNA expression of RANK, TRAP and NFATc1 in the OSCAR⁺ cells sorted from BMs by FACS from the OVX mice pretreated with D-Asp₈ or PBS followed by the administration of (D-Asp₈)-liposome-antagomir-148a at 48 h after administration. Note: The miR-148a expression levels in each group were normalized by the U6 expression level. The knockdown of the miR-148a was calculated by comparing the miR-148a expression levels in the antagomir-148a group to those in the appropriate non-sense antagomir group. The mRNA expression levels of RANK, TRAP and NFATc1 were normalized by the GAPDH mRNA expression level. The relative fold change was calculated by comparing the mRNA expression levels in the antagomir-148a group to those in the appropriate non-sense antagomir group. The dose of antagomir-148a or non-sense antagomir was 8 mg/kg in the corresponding treatment group. The data were presented as the mean ± s.d., n = 6 per group. *P < 0.05 for a comparison of OSCAR⁺ cells with the OSCAR⁻ cells in (a) & (c), and for a comparison of antagomir-148a treated group with non-sense antagomir treated group in (b) & (d).

group (data not shown), indicating the conjugation of D-Asp₈ has no influence on the capacity of liposome on protection from endogenous nucleases-mediated degradation. Thus, the (D-Asp₈)-liposome could be a cargo for delivering miRNA modulators *in vivo*.

Previously published studies have shown that D-Asp₈ could preferentially bind to highly crystallized hydroxyapatite [12–14], which is the physicochemical characterization of bone resorption surfaces [12,15], implying its potential as targeting moiety to

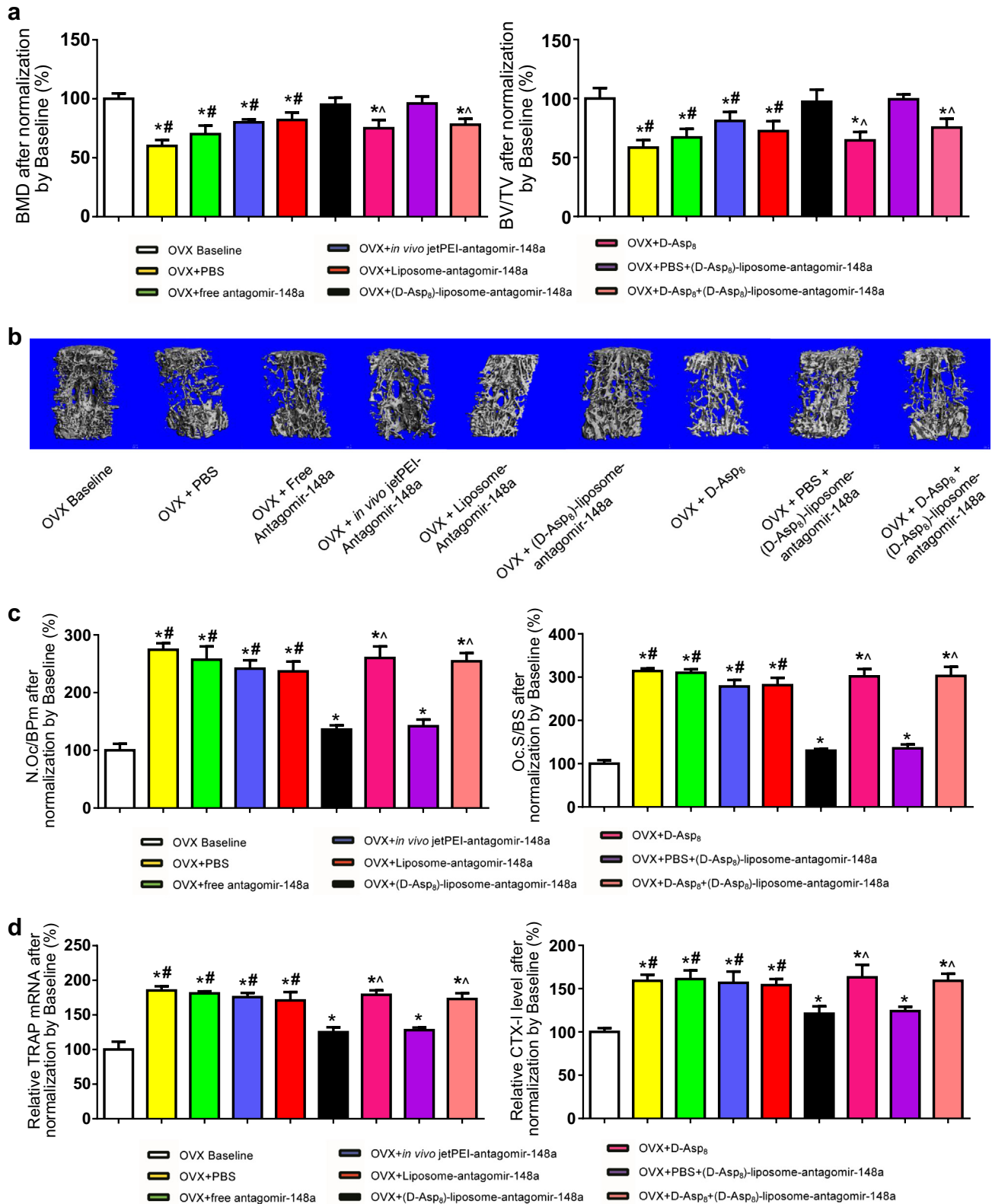


Fig. 6. Therapeutic effects of antagomir-148a delivered by (D-Asp₈)-liposome on OVX mice. (a) Micro-CT analysis for the BMD (bone mineral density) and BV/TV (relative bone volume) of the trabecular bone in 5th lumbar body (LV5) from the ovariectomized (OVX) mice at baseline before treatment initiation, or the OVX mice administrated with PBS, free antagomir-148a, *in vivo* jetPEI-antagomir-148a, liposome-antagomir-148a or (D-Asp₈)-liposome-antagomir-148a, or the OVX mice treated with D-Asp₈ alone, or the mice pretreated with D-Asp₈ or PBS followed by the administration of (D-Asp₈)-liposome-antagomir-148a after 6-week treatments. (b) Representative three-dimensional reconstructed images for the trabecular bone in LV5 from each group after 6-week treatments. (c) Bone histomorphometry analysis for N.Oc/BPm (osteoclast number, mm⁻¹) and Oc.S/BS (osteoclast surface, %) in LV5 from each group after 6-week treatments. (d) Real-time PCR (RT-PCR) analysis for the intra-osseous TRAP (Tartrate-resistant Acid Phosphatase) mRNA level (left) and enzyme-linked immuno sorbent assay (ELISA) for the serum CTX-I (C-Terminal Telopeptides Type I Collagen) level (right) from each group after 6-week treatments. Note: The data were presented as the mean \pm s.d., n = 6 per group. *P < 0.05 versus OVX baseline Group, #P < 0.05 versus OVX + (D-Asp₈)-liposome-antagomir-148a Group, ^P < 0.05 versus OVX + D-Asp₈ + (D-Asp₈)-liposome-antagomir-148a Group.

approach the bone resorption surfaces. Our current data from TRAP staining following bone histomorphometry analysis further validated our published findings that D-Asp₈ moiety could bind to bone resorption surfaces [15], as evidenced by the rhodamine B labeling at the bone resorption surface after the mice were treated with rhodamine B-conjugated D-Asp₈. Furthermore, at the tissue level, the data from biophotonic imaging and microplate reader analysis *in vivo* suggested that D-Asp₈ moiety could facilitate delivering antagomir-148a encapsulated in liposome to bone tissues and reducing the exposure of antagomir-148a to non-skeletal tissues, as evidenced by the strongest fluorescence signal of the FAM-labeled antagomir-148a in bone tissues and relative lower fluorescence signal in non-skeletal tissues in the (D-Asp₈)-liposome-antagomir-148a group when compared to the other treatment groups (the free antagomir-148a group, *in vivo* jetPEI-antagomir-148a group and liposome-antagomir-148a group). In addition, at the cellular level, the data from immunohistochemistry analysis indicated that D-Asp₈ moiety could facilitate delivering antagomir-148a encapsulated in liposome to osteoclasts, as suggested by significantly more instances of co-localization of FAM-labeled antagomir-148a with OSCAR⁺ cells in (D-Asp₈)-liposome-antagomir-148a group when compared to the other treatment groups. For the mechanistic understandings, the data from immunohistochemistry analysis indicated that the targeting mechanism could be dependent on the interaction between D-Asp₈ and bone resorption surfaces, as evidenced by the notable reduction in the instances of co-localization of FAM-labeled antagomir-148a with OSCAR⁺ cells in the mice with D-Asp₈ pretreatment. Taken together, the above data suggested that D-Asp₈ moiety could specifically bind to bone resorption surfaces and, thus, facilitate selectively delivering antagomir-148a encapsulated in liposome to the mature osteoclasts and osteoclast progenitors nearby.

In this study, almost 80% knockdown efficiency in osteoclasts was achieved at the antagomir-148a dose of 8 mg/kg and over 50% knockdown efficiency was maintained for about 1 week in the (D-Asp₈)-liposome-antagomir-148a group, indicating that 8 mg/kg of antagomir-148a is enough for the efficient knockdown of miR-148a in osteoclasts when it was delivered by (D-Asp₈)-liposome. However, lower miR-148 knockdown efficiency and shorter persistence period at the same dose was found when the antagomir-148a was delivered by either *in vivo* jetPEI or liposome alone, respectively. This difference could be attributed to the lack of targeted mechanism for *in vivo* jetPEI or liposome to deliver antagomir-148a to osteoclasts selectively and efficiently. In addition, the real-time PCR data further demonstrated that D-Asp₈ moiety could facilitate delivering antagomir-148a encapsulated in liposome to significantly knockdown miR-148a expression in osteoclasts, as evidenced by the remarkable decrease in miR-148a expression within bone marrow-derived OSCAR⁺ cells isolated by FACS in (D-Asp₈)-liposome group when compared to the other treatment groups. The cell-selective knockdown of miR-148a was corresponding to the above bone tissue-selective distribution and osteoclast-selective delivery of antagomir-148a by (D-Asp₈)-liposome. Further, the selective knockdown of the miR-148a in OSCAR⁺ cells by (D-Asp₈)-liposome-antagomir-148a was abolished after pre-treatment with D-Asp₈, which could be explained by the aforementioned D-Asp₈-bone resorption surfaces interaction mechanism.

The micro-CT, bone histomorphometry, real time PCR and ELISA data jointly indicated that D-Asp₈ moiety could facilitate delivering antagomir-148a encapsulated in liposome to inhibit bone resorption and attenuate the deterioration in trabecular architecture after ovariectomy, as evidenced by the significant attenuation of the decreases in BMD and BV/TV and the increases in N.Oc/BPm, Oc.S/BS, intra-osseous TRAP mRNA and serum CTX-I level in the (D-Asp₈)-liposome-antagomir-148a group at a dose of 8 mg/kg

when compared to the other treatment groups. However, the therapeutic administration of free antagomir-148a should reach a much higher dose (80 mg/kg) in the previous study [2]. It suggested that D-Asp₈-liposome could remarkably facilitate achieving the therapeutic effect of antagomir-148a even at a relative low dose. More impressively, the inhibitory effects on bone resorption and preventive effects on trabecular deterioration of (D-Asp₈)-liposome-antagomir-148a were abolished by D-Asp₈ pretreatment. Consistently, it could be explained by the targeted mechanism through the interaction between bone resorption surfaces and D-Asp₈. Taken together, the D-Asp₈ could facilitate antagomir-148a encapsulated in liposome to inhibit osteoclastic bone resorption *in vivo*.

Considering that microRNAs may play crucial role in regulating the physiology of various organs [32–34], the safety concern about the application of microRNA modulator therapy should be taken seriously. In our study, the *in vivo* data from biophotonic imaging and liver/kidney-related biochemistry assays consistently implied that D-Asp₈ could facilitate reducing antagomir-148a exposure to liver and kidney with minimal toxicity on them.

We have previously developed a (DSS)₆-based osteoblast-targeted delivery system for specifically approaching bone formation surface to target osteogenic cells [15], thus providing a tool for RNA interference-based bone anabolic strategies. In this study, we generated the osteoclast-targeted delivery system, *i.e.* (D-Asp₈)-liposome, using D-Asp₈ as the target moiety to facilitate microRNA modulators approaching bone resorption surfaces to target osteoclastic cells. It would provide another useful tool for delivering microRNA modulators to osteoclasts. The cell-targeted mechanism depends on the exposure of hydroxyapatite in different crystallization status to the specific oligo-peptides moiety. Collectively, it indicates that specifically approaching bone remodeling surfaces (either bone formation surfaces or bone resorption surfaces) could be a feasible strategy for cell-targeted delivery of therapeutic siRNA or microRNA modulators.

5. Conclusions

In summary, our study demonstrated that the D-Asp₈ could facilitate miRNA modulators encapsulated in DOTAP-based liposome specifically approaching bone-resorption surfaces to selectively target osteoclast to regulate osteoclast function. (D-Asp₈)-liposome could be a promising osteoclast-targeting delivery system to facilitate clinical translation of miRNA modulators in treating osteoclast-dysfunction-induced skeletal diseases.

Acknowledgments

The statistical analysis in this study was performed by a contract service from Bioinformedicine (San Diego, CA, USA, <http://www.bioinformedicine.com/index.php>). This work was supported by the Faculty Research Grant of Hong Kong Baptist University (FRG2/13-14/006), the Hong Kong General Research Fund (12102914 and HKBU 478312), Interdisciplinary Research Matching Scheme (IRMS) of Hong Kong Baptist University (RC-IRMS/13-14/02 and RC-IRMS/13-14/03), the Research Committee of Hong Kong Baptist University (30-12-286 and FRG2/12-13/027), the Science and Technology Innovation Commission of Shenzhen Municipality (SCM-2013-SZTIC-001), Natural Science Foundation Council (81272045 and 81401833).

Appendix A. Supplementary data

Supplementary data related to this article can be found at <http://dx.doi.org/10.1016/j.biomaterials.2015.02.007>.

Author contributions

Ge Zhang, Aiping Lu and Baosheng Guo supervised the whole project and wrote most of the manuscript. Jin Liu, Lei Dang and Defang Li performed the major experiments and prepared the manuscript in equal contribution. Xiaojuan He, Heng Wu provided the technical support. Airong Qian, Zhijun Yang, Doris. W. T. Au, Michael. W. L. Chiang, Bao-Ting Zhang, Quanbin Han, Kevin K. M. Yue, Hongqi Zhang, Changwei Lv, Xiaohua Pan, Jiake Xu, Zhaoxiang Bian, Peng Shang, Weihong Tan and Zicai Liang provided their professional expertise.

References

- [1] Edwards JR. Osteoclasts: malefactors of disease and targets for treatment. *Discov Med* 2012;13(70):201–10.
- [2] Cheng P, Chen C, He HB, Hu R, Zhou HD, Xie H, et al. miR-148a regulates osteoclastogenesis by targeting V-maf musculoaponeurotic fibrosarcoma oncogene homolog B. *J Bone Min Res* 2013;28(5):1180–90.
- [3] Kagiya T, Nakamura S. Expression profiling of microRNAs in RAW264.7 cells treated with a combination of tumor necrosis factor alpha and RANKL during osteoclast differentiation. *J Periodontol Res* 2013;48(3):373–85.
- [4] Zhang J, Zhao H, Chen J, Xia B, Jin Y, Wei W, et al. Interferon-beta-induced miR-155 inhibits osteoclast differentiation by targeting SOCS1 and MITF. *FEBS Lett* 2012;586(19):3255–62.
- [5] Gong M, Ma J, Guillemette R, Zhou M, Yang Y, Yang Y, et al. miR-335 inhibits small cell lung cancer bone metastases via IGF-IR and RANKL pathways. *Molecular cancer research*. MCR 2014;12(1):101–10.
- [6] Rossi M, Pitari MR, Amodio N, Di Martino MT, Conforti F, Leone E, et al. miR-29b negatively regulates human osteoclastic cell differentiation and function: implications for the treatment of multiple myeloma-related bone disease. *J Cell Physiol* 2013;228(7):1506–15.
- [7] Janssen HL, Reesink HW, Lawitz EJ, Zeuzem S, Rodriguez-Torres M, Patel K, et al. Treatment of HCV infection by targeting microRNA. *N Engl J Med* 2013;368(18):1685–94.
- [8] Stenvang J, Petri A, Lindow M, Obad S, Kauppinen S. Inhibition of microRNA function by anti-miR oligonucleotides. *Silence* 2012;3(1):1.
- [9] Nana-Sinkam SP, Croce CM. Clinical applications for microRNAs in cancer. *Clin Pharmacol Ther* 2013;93(1):98–104.
- [10] Hydbring P, Badalian-Very G. Clinical applications of microRNAs. *F1000 Res* 2013;2:136.
- [11] Kamaly N, Xiao Z, Valencia PM, Radovic-Moreno AF, Farokhzad OC. Targeted polymeric therapeutic nanoparticles: design, development and clinical translation. *Chem Soc Rev* 2012;41(7):2971–3010.
- [12] Wang D, Miller SC, Shlyakhtenko LS, Portillo AM, Liu XM, Papangkorn K, et al. Osteotropic peptide that differentiates functional domains of the skeleton. *Bioconjug Chem* 2007;18(5):1375–8.
- [13] Wang D, Sima M, Mosley RL, Davda JP, Tietze N, Miller SC, et al. Pharmacokinetic and biodistribution studies of a bone-targeting drug delivery system based on N-(2-hydroxypropyl)methacrylamide copolymers. *Mol Pharm* 2006;3(6):717–25.
- [14] Wang D, Miller S, Sima M, Kopeckova P, Kopecek J. Synthesis and evaluation of water-soluble polymeric bone-targeted drug delivery systems. *Bioconjug Chem* 2003;14(5):853–9.
- [15] Zhang G, Guo B, Wu H, Tang T, Zhang BT, Zheng L, et al. A delivery system targeting bone formation surfaces to facilitate RNAi-based anabolic therapy. *Nat Med* 2012;18(2):307–14.
- [16] Jensen DK, Jensen LB, Koocheki S, Bengtson L, Cun D, Nielsen HM, et al. Design of an inhalable dry powder formulation of DOTAP-modified PLGA nanoparticles loaded with siRNA. *Journal of controlled release. Off J Control Release Soc* 2012;157(1):141–8.
- [17] Gao J, Sun J, Li H, Liu W, Zhang Y, Li B, et al. Lyophilized HER2-specific PEGylated immunoliposomes for active siRNA gene silencing. *Biomaterials* 2010;31(9):2655–64.
- [18] Peer D, Park EJ, Morishita Y, Carman CV, Shimaoka M. Systemic leukocyte-directed siRNA delivery revealing cyclin D1 as an anti-inflammatory target. *Science* 2008;319(5863):627–30.
- [19] Mendonca LS, Firmino F, Moreira JN, Pedroso de Lima MC, Simoes S. Transferrin receptor-targeted liposomes encapsulating anti-BCR-ABL siRNA or asODN for chronic myeloid leukemia treatment. *Bioconjug Chem* 2010;21(1):157–68.
- [20] Santos AO, da Silva LC, Bimbo LM, de Lima MC, Simoes S, Moreira JN. Design of peptide-targeted liposomes containing nucleic acids. *Biochim Biophys Acta* 2010;1798(3):433–41.
- [21] Cardoso A, Trabulo S, Moreira JN, Duzgunes N, de Lima MC. Targeted liposomes for siRNA delivery. *Methods Enzym* 2009;465:267–87.
- [22] Ishikawa S, Arase N, Suenaga T, Saita Y, Noda M, Kuriyama T, et al. Involvement of FcRgamma in signal transduction of osteoclast-associated receptor (OSCAR). *Int Immunol* 2004;16(7):1019–25.
- [23] Kim N, Takami M, Rho J, Josien R, Choi Y. A novel member of the leukocyte receptor complex regulates osteoclast differentiation. *J Exp Med* 2002;195(2):201–9.
- [24] Naylor K, Eastell R. Bone turnover markers: use in osteoporosis. *Nat Rev Rheumatol* 2012;8(7):379–89.
- [25] Liu XY, Ruan LM, Mao WW, Wang JQ, Shen YQ, Sui MH. Preparation of RGD-modified long circulating liposome loading matrine, and its in vitro anti-cancer effects. *Int J Med Sci* 2010;7(4):197–208.
- [26] Harris TJ, Green JJ, Fung PW, Langer R, Anderson DG, Bhatia SN. Tissue-specific gene delivery via nanoparticle coating. *Biomaterials* 2010;31(5):998–1006.
- [27] Yokogawa K, Toshima K, Yamoto K, Nishioka T, Sakura N, Miyamoto K. Pharmacokinetic advantage of an intranasal preparation of a novel anti-osteoporosis drug, L-Asp-hexapeptide-conjugated estradiol. *Biol Pharm Bull* 2006;29(6):1229–33.
- [28] Wang X, Guo B, Li Q, Peng J, Yang Z, Wang A, et al. miR-214 targets ATF4 to inhibit bone formation. *Nat Med* 2013;19(1):93–100.
- [29] Zhang G, Sheng H, He YX, Xie XH, Wang YX, Lee KM, et al. Continuous occurrence of both insufficient neovascularization and elevated vascular permeability in rabbit proximal femur during inadequate repair of steroid-associated osteonecrotic lesions. *Arthritis Rheum* 2009;60(10):2966–77.
- [30] Guo B, Zhang B, Zheng L, Tang T, Liu J, Wu H, et al. Therapeutic RNA interference targeting CKIP-1 with a cross-species sequence to stimulate bone formation. *Bone* 2014;59:76–88.
- [31] Parfitt AM, Drezner MK, Glorieux FH, Kanis JA, Malluche H, Meunier PJ, et al. Bone histomorphometry: standardization of nomenclature, symbols, and units. Report of the ASBMR histomorphometry Nomenclature Committee. *J Bone Min Res* 1987;2(6):595–610.
- [32] Chang TC, Mendell JT. microRNAs in vertebrate physiology and human disease. *Annu Rev Genomics Hum Genet* 2007;8:215–39.
- [33] Sayed D, Abdellatif M. MicroRNAs in development and disease. *Physiol Rev* 2011;91(3):827–87.
- [34] Li M, Marin-Muller C, Bharadwaj U, Chow KH, Yao Q, Chen C. MicroRNAs: control and loss of control in human physiology and disease. *World J Surg* 2009;33(4):667–84.